

SEVERAL DESIGN ISSUES ON THE TUNABLE ELECTROMAGNETIC VIBRATION ABSORBER

Jie Liu*, Kefu Liu

Department of Mechanical Engineering, Lakehead University
955 Oliver Road, Thunder Bay, Ontario, Canada P7B 5E1

ABSTRACT

This paper addresses several design issues related to a newly developed electromagnetic vibration absorber (EMVA). The EMVA consists of a clamped-clamped aluminum beam and a permanent magnet that is embedded in the centre of the beam and placed between two poles of a C-shaped electromagnet. By varying the current of the electromagnet, stiffness of the EMVA can be adjusted instantaneously. First a simplified equation is proposed to compute the flux density distribution in the gap of the electromagnet. The approximation error caused by the simplification is investigated. Second, the effect of cross-sectional shapes of the permanent magnet on the variable magnetic stiffness and the constant magnetic stiffness is examined. Finally, the effect of the gap spaces of the electromagnet on the variable magnetic stiffness is studied.

1. Introduction

Tunable vibration absorbers belong to the family of semi-active control systems. Nowadays, semi-active control systems are attracting more and more research interests in the field of vibration control, since they combine the advantages of both passive and active control systems. Generally, the mechanical properties of the semi-active systems, such as the stiffness and/or the damping value, can be adjusted based on the feedback from the measured response and/or the excitation. Several variable stiffness vibration absorbers have been proposed. Stiffness variation of the device reported in [1] was achieved by varying the effective number of coils in a helical spring used as the absorber stiffness. A vibration absorber developed in [2] consists of a flexible cantilever beam attached by a mass at its free end. By varying the length of the beam, the absorber frequency can be varied. A variable stiffness device proposed in [3] has four coil springs arranged in a planar rhombus configuration. The aspect ratio of the rhombus configuration can be varied by a linear electromechanical actuator to achieve a continuous variation of the absorber stiffness. In [4], a variable stiffness absorber similar to the one developed in [2] was used to compare two different tuning algorithms. It is noted that all the above tunable devices involve an electro-mechanically driven system. As a result, a slow reaction speed may become the main concern for these types of stiffness control devices. Alternatively, damping is sometimes added to the absorber systems to prevent resonance or to improve the effective bandwidth of operation. Damping value can be made on-line adjustable by utilizing a variable-orifice valve to alter the resistance to the flow of a conventional hydraulic fluid damper [5, 6]. Friction dampers have also been widely studied as another approach in semi-active vibration control [7, 8]. Most noticeably, electro-rheological or magneto-rheological dampers feature a broad-bandwidth modulation of the damping characteristics through the variation of an electrical or magnetic field [9-11]. However, when adding the damping into the system, the performance of the absorber at the design frequency is sacrificed.

Over the past decade, various devices based on magnetism or electromagnetism have been used to suppress vibration. The electromagnetic servomechanism developed in [12] consists of a pair of electromagnets and a lever. When the electromagnets are energized, interacting forces are produced between the electromagnets and the lever. The device was used in the study of active vibration control. In [13], permanent magnets were used to build an extremely soft spring for the purpose of vibration isolation. A hybrid-type active vibration isolation system developed in [14] uses both electromagnetic and pneumatic forces. In [15], an electromagnetic device was designed to parametrically excite the experimental beam. The phenomenon of eddy current has been explored to develop magnetic dampers [16-18].

* Corresponding author, Tel: +1-807-766-7102, Fax: +1-807-343-8928, Email: jliu1235@lakeheadu.ca

In [19], an electromagnetic vibration absorber (EMVA) was proposed by the authors of this paper. Similar to the devices in [1-4], the EMVA is a variable stiffness one. However, a notable difference is that the EMVA is non-contact, with non-mechanical motion, and its stiffness can be changed instantly. Furthermore, it is tunable on-line. The characterization and application of the EMVA were presented in [19]. This paper reports some follow-up study results: several issues related to the design of the EMVA. The rest of the paper is organized as follows: In Section 2, the EMVA is introduced. In Section 3, design issues of the EMVA are discussed. Finally, in Section 4, the conclusions of the study are given.

2. Electromagnetic Vibration Absorber

Figure 1 shows a photograph of the developed electromagnetic vibration absorber attached to a primary system. The entire experimental system consists of three subsystems: EMVA, primary system, and computer control system. As schematically shown in Fig. 2, the EMVA comprises a clamped-clamped aluminum beam (1) and a permanent magnet (PM) (2) that is embedded in the centre of the beam and placed between two poles of an electromagnet (3). The electromagnet is constructed by winding Gauge 18 copper wire around a C-shaped steel core. The permanent magnet plays a dual role: acting as an absorber mass and forming a variable magnetic spring by interacting with the electromagnet through varying the direct current (DC) of the electromagnetic coils. The primary system (4) is an aluminum slab supported by an aluminum plate on each side, acting like a single degree-of-freedom (DOF) system. The electromagnet is fastened to the slab by two brackets, forming part of the primary mass. A small permanent magnet (5) is glued on an aluminum bar that is clamped to the primary mass. This permanent magnet interacts with an electromagnetic shaker (6) to generate a non-contact exciting force. The purpose of adding the aluminum bar between the permanent magnet and the primary mass is to minimize the interference of the magnetic field generated by the forcing electromagnet and the one generated by the absorber electromagnet. The parameters of the system are summarized in Table 1.

The computer control system includes the instrumentation and a Pentium III computer equipped with a Data Acquisition (DAC) Board DS1102 (dSpace). The response of the absorber mass is measured by an accelerometer, and conditioned via a charge amplifier. Subsequently, the signal is input into the computer through an analog to digital (A/D) channel of the DAC board. ControlDesk (dSpace) provides the interface between Matlab, Simulink and DS1102. A Simulink model is developed to implement on-line tuning. The sampled data are first stored in an S-function named "Buffer" until a specified data length (1024/2048) is reached. Then the data are passed to an S function named "FFT" where the Fast Fourier Transform (FFT) is conducted and the peak frequency in the FFT spectrum is determined. Using the measured exciting frequency, the desired coil current is computed and sent to a current regulator board via a digital to analog channel (D/A). The output of the board supplies the desired amplitude of the direct current to the electromagnetic coils. The exciting signal is generated by a subsystem within the Simulink model and sent to a power amplifier via a D/A channel. The output of the amplifier drives the electromagnetic shaker to excite the primary system.

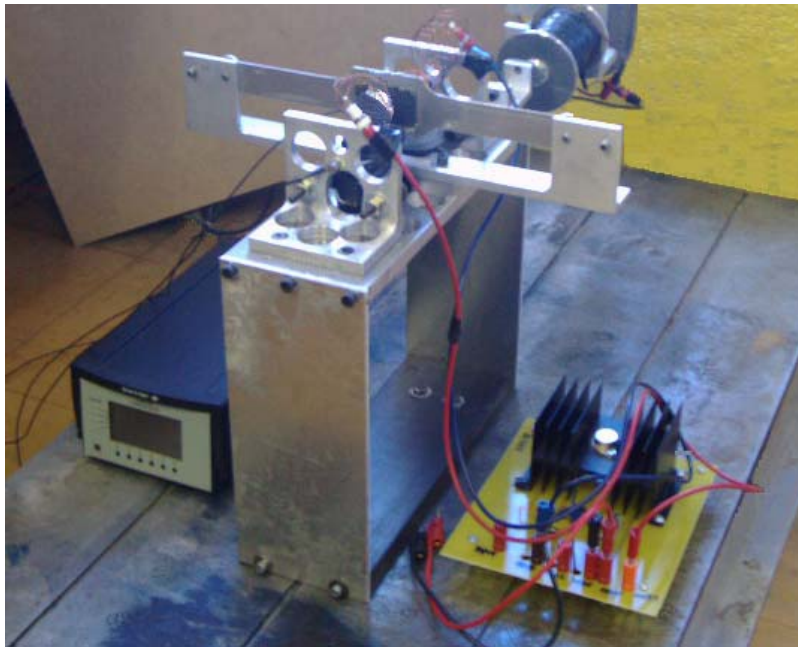


Figure 1. Photograph of the experimental setup.

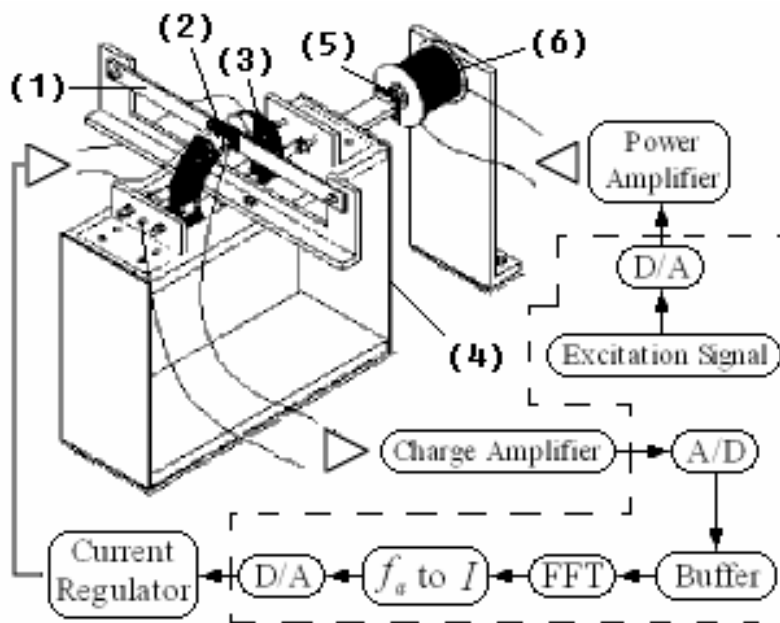


Figure 2. Schematic of the entire experimental system.

Table 1: System parameters

Symbol	Description	Value
m_a	Absorber mass	0.151 kg
m	Primary mass	3.074 kg
c_a	Damping coefficient of the absorber system	0.18 Ns/m
c	Damping coefficient of the primary system	3.71 Ns/m
R_1	Inner radius of the electromagnetic coils	11 mm
R_2	Outer radius of the electromagnetic coils	20 mm
L	Circumference of the electromagnet	314.16 mm
N	Turns of the coils	784
μ_0	Magnetic permeability of free space	$4\pi \times 10^{-7}$ H/m
δ	The gap space between two pole faces of the electromagnet	42.0 mm
l	Length of the PM	48.0 mm
w	Height of the PM	22.0 mm
h	Thickness of the PM	10.0 mm

3. Design Issues Related to the EMVA

As shown in Fig. 3, three springs are involved in the EMVA, namely, constant spring k_{c1} caused by the absorber beam, constant spring k_{c2} caused by the interaction between the permanent magnet and the core of the electromagnet, and variable spring k_v caused by the interaction between the permanent magnet and electromagnet.

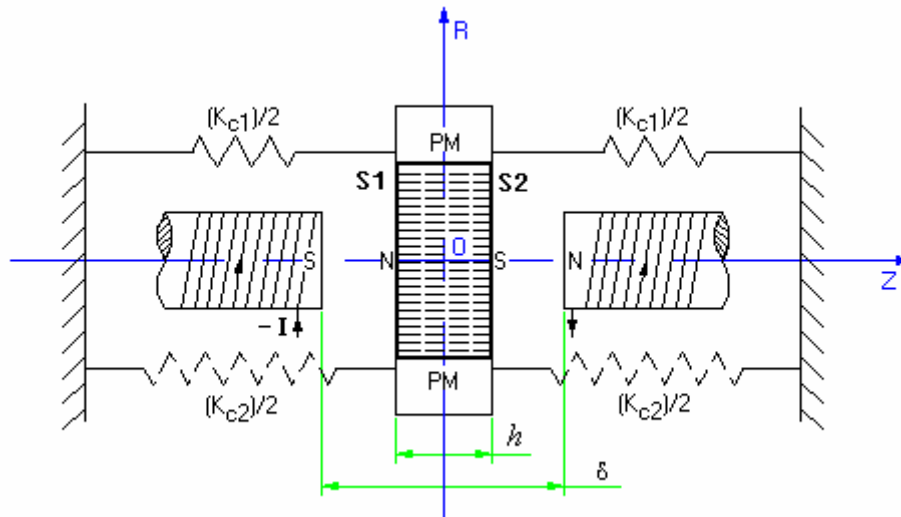


Figure 3. Three springs involved in the EMVA.

3.1 A Simplified Equation for the Determination of the Flux Density of the Electromagnet

To determine the magnetic stiffness, first the magnetic field between the poles of the electromagnet needs to be found. In [19], it was done by using the fundamental theory of electromagnetism. It involves numerically

solving a triple integration. In what follows, a simplified numerical approach is proposed and the approximation errors caused by this simplification are investigated. First the method used in [19] is briefly introduced. The analysis strategy employed in [19] first computes the flux density of one pole of the electromagnet. In order to do it, the coils are modeled as a current carrying hollow cylinder with an inner radius R_1 , an outer radius R_2 , and a length L as shown in Fig. 4. The hollow cylinder is composed of infinite numbers of circular current loops. According to the Biot-Salvart law, the flux density in the axial direction z of a circular current loop with a radius a (Fig. 5) is given as [20]:

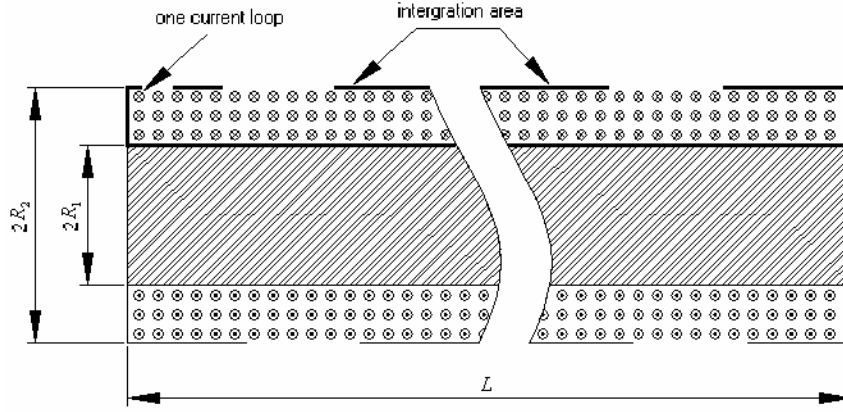


Figure 4. Current carrying hollow cylinder

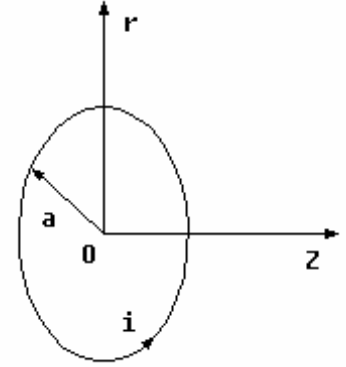


Figure 5. Circular current loop

$$B_l = \frac{\mu_0 i}{2\pi} \frac{1}{[(a+r)^2 + z^2]^{1/2}} \left[E_2 \frac{a^2 - r^2 - z^2}{(a-r)^2 + z^2} + E_1 \right], \quad (1)$$

where E_1 and E_2 are the complete elliptic integrals of the first and second kind, respectively, and they are of the forms:

$$E_1 = \int_0^{\pi/2} \left[1 - \frac{4ar}{(a+r)^2 + z^2} \sin^2 \theta \right]^{-1/2} d\theta, \quad E_2 = \int_0^{\pi/2} \left[1 - \frac{4ar}{(a+r)^2 + z^2} \sin^2 \theta \right]^{1/2} d\theta \quad (2)$$

The axial contribution of the magnetic flux of the cylinder can be found by integrating Eq. (1) in both the radial and axial directions

$$B_c = \int_{R_1}^{R_2} \int_0^L B_l(a, r, z + \lambda) d\lambda da \quad (3)$$

where B_c is the axial magnetic flux density from one pole of the current carrying cylinder, with the origin located at the centre of the pole face. Note that in Eq. (3), B_l is defined by Eq. (1) with the loop current i given by

$$i = \frac{NI}{(R_2 - R_1)L} \quad (4)$$

where I is the coil current.

The solution of Eq. (3) involves a triple integration which must be done numerically (note that finding E_1, E_2 requires one integration). To simplify the computation, the hollow cylinder may be replaced by a current carrying cylindrical sheet with a radius R . This way, Eq. (3) becomes

$$B_c = \int_0^L B_l(R, r, z + \lambda) d\lambda \quad (5)$$

The loop current i should be substituted by

$$i = \frac{NI}{L} \quad (6)$$

The flux density B_c computed by Eq. (3) or Eq. (5) is the one without the effect of the core of the electromagnet. A ferromagnetic core can significantly magnify the magnetic strength. The effect is included by considering the relative permeability and the flux leakage,

$$B_{em} = \mu_r / \gamma B_c \quad (7)$$

where B_{em} is the flux density from one pole of the coils, μ_r is the relative permeability of the steel core, and γ is the leakage factor. The term μ_r / γ is normally determined experimentally. In [19], using a DC magnetometer, an experiment was conducted and it was found that for the present setup, $\mu_r / \gamma = 27.3$.

With the flux density from one pole of the electromagnet available, the total magnetic flux densities between the two poles of the electromagnet can then be found by superposition. Using the parameters given in Table 1 and $I = 1.5$ A, Fig. 6 shows a comparison of the result based on Eq. (3) and that based on Eq. (5). To use Eq. (5), the radius R is determined by

$$R = \sqrt{\frac{R_1^2 + R_2^2}{2}} \quad (8)$$

This R divides the cylinder into two cylinders that have the same cross-sectional areas. It can be seen that both Eqs. (3) and (5) give a similar distribution. To quantitatively compare the difference of the two results, an error index is defined as

$$\varepsilon = \frac{\sum_{i=1}^{51} \sum_{j=1}^{21} |B_{em}^1(r_i, z_j) - B_{em}^2(r_i, z_j)|}{\sum_{i=1}^{51} \sum_{j=1}^{21} |B_{em}^1(r_i, z_j)|} \quad (9)$$

where B_{em}^1 is the total flux density based on Eq. (3), B_{em}^2 the one based on Eq. (5), z_j is varied from 0 to .02 m in a step of .001 m and r_i is varied from 0 to .05 m in a step of .001 m. The following five cases are considered: (1) $R_1 = .015$ m, $R_2 = .017$ m, (2) $R_1 = .014$ m, $R_2 = .018$ m, (3) $R_1 = .011$ m, $R_2 = .020$ m, (4) $R_1 = .009$ m, $R_2 = .021$ m, (5) $R_1 = .006$ m, $R_2 = .022$ m. Note that the five cases are chosen in a way such that $R = .0161$ m and $R_2 - R_1$ is increased. Fig. 7 compares the results in two ways. Fig. 7(a) gives $B_{em}^1 - B_{em}^2$ where B_{em}^1 corresponds to case three. Fig. 7(b) shows the error index ε for the five cases. It is noted that the error mainly occurs at the pole faces and in the radial direction around the radius R and the error increases with the increase

of $R_2 - R_1$.

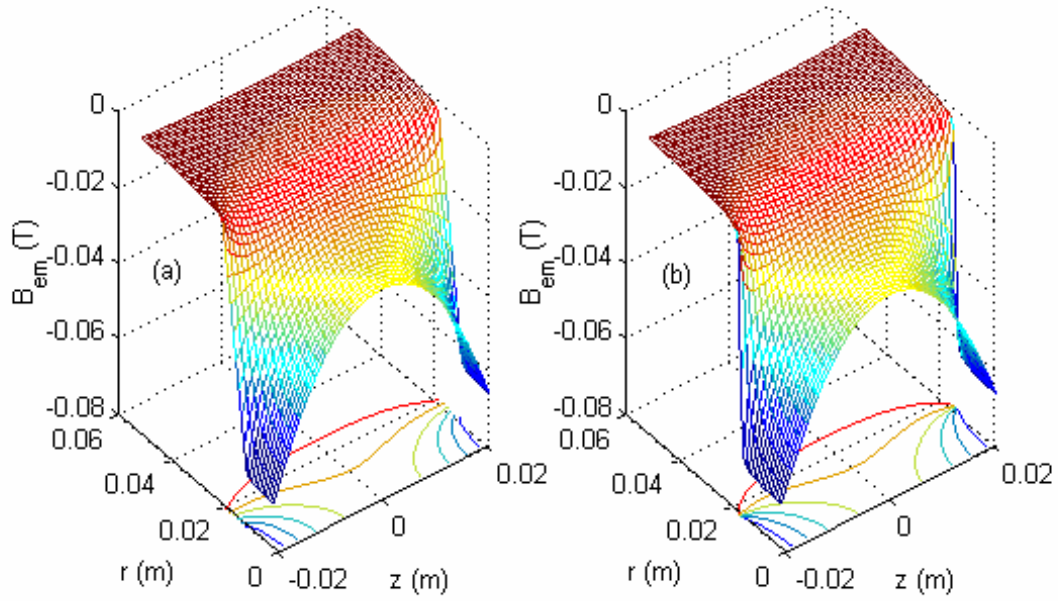


Figure 6. The magnetic flux density of the electromagnet for $I = 1.5$ A: (a) based on Eq. (3); (b) based on Eq. (5)

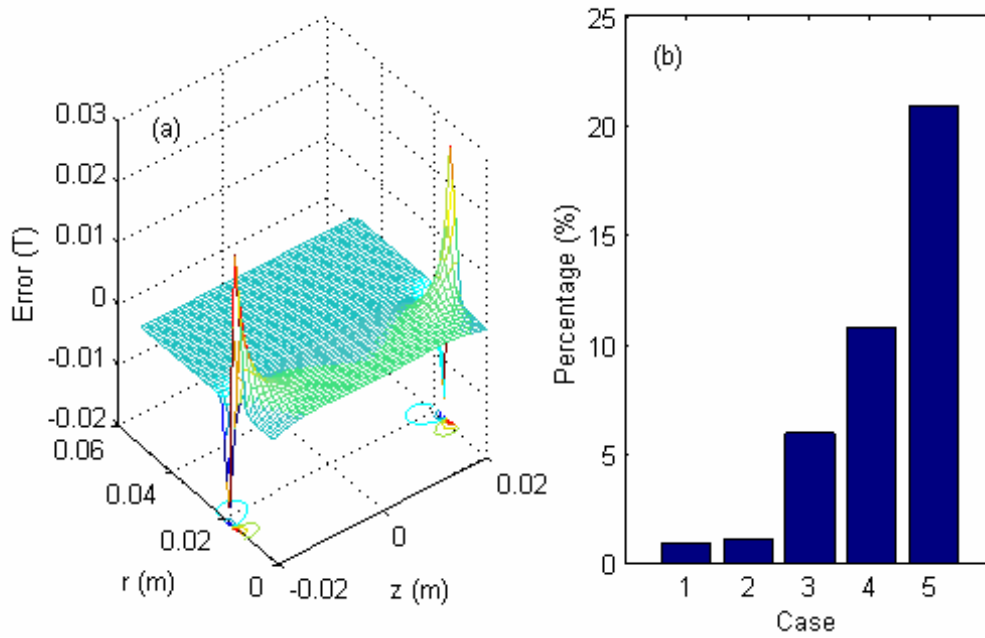


Figure 7. Comparison of B_{em}^1 and B_{em}^2 ; (a) $B_{em}^1 - B_{em}^2$; (b) ε defined by Eq. (9)

3.2 Effect of Different Cross-Sectional Shapes of PM on k_v

With the magnetic field distributions of the electromagnet available, the interacting force between the electromagnet and the PM can be found by [19, 20]

$$F = M \left(\int_{S_1} B_{em1} dS - \int_{S_2} B_{em2} dS \right) \quad (10)$$

where M is the magnetization of the PM, B_{em1} and B_{em2} are the flux density on the pole faces S_1 and S_2 of the PM, respectively. The magnetization M for the PM used in the apparatus was experimentally found to be $M = 395.8 \text{ kAm}^{-1}$ [19]. Figure 8 shows the curves of the electromagnetic force versus the displacement of the PM for four different coil currents. As shown in the figure, within the range of $[-.01, .01] \text{ m}$, the force-displacement relationship is close to linear. The linearized curves are shown in the figure as well, and their slopes are the electromagnetic stiffness k_v . It is also understandable that when positive currents are applied, similar curves with positive slopes are obtained, which results in the positive electromagnetic stiffness k_v .

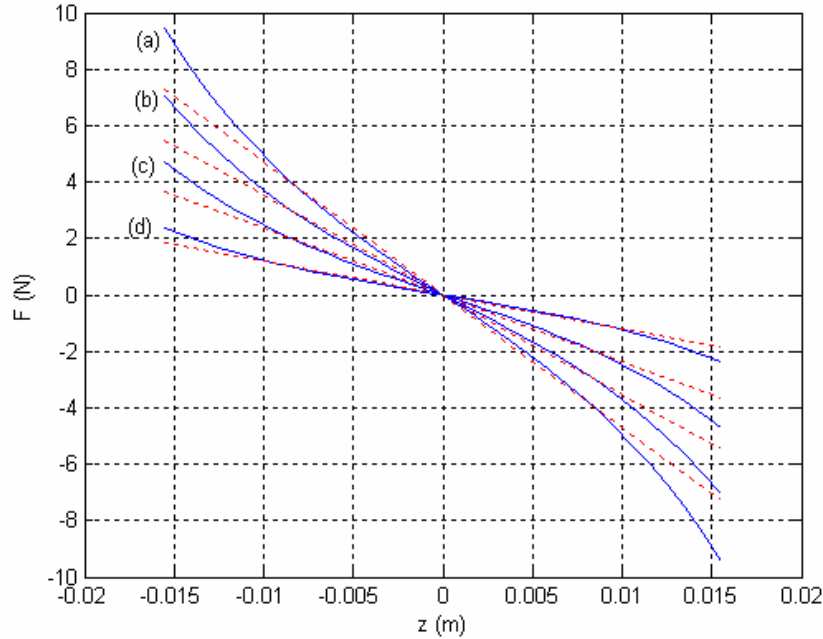


Figure 8. Interaction force versus the displacement of the PM: (a) $I = -2.0 \text{ A}$, (b) $I = -1.5 \text{ A}$, (c) $I = -1.0 \text{ A}$, (d) $I = -0.5 \text{ A}$: solid line, analytical; dotted line, linearized.

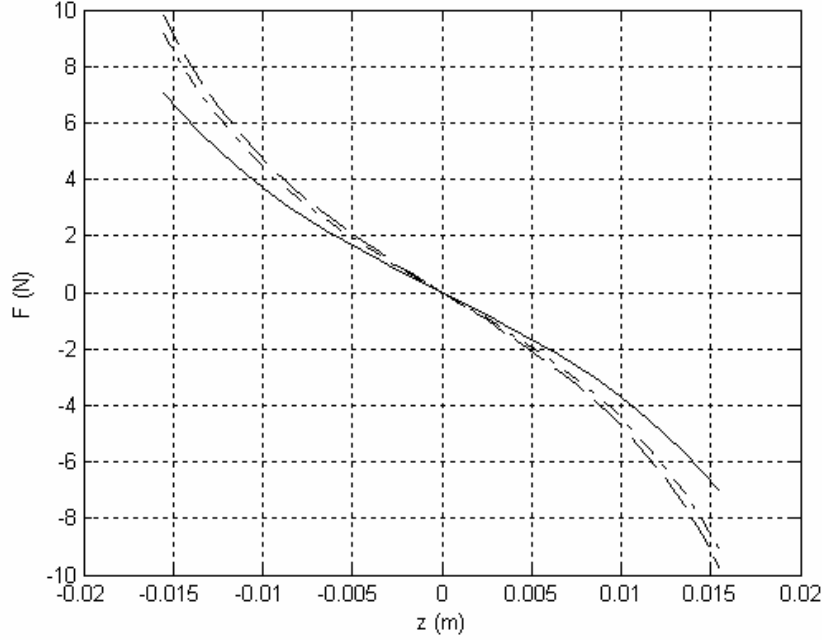


Figure 9. Interaction force versus the displacement of the PM for three different shapes of the PM: solid line, rectangular; dashdot line, square; dashed line, round.

The present EMVA uses a rectangular shape PM because it is readily available. A natural question arises: how does a cross-sectional shape of the PM affect k_v ? To understand it, the interacting forces are computed using two more cross-sectional shapes: square and round. In the both cases, the dimension is chosen such that all the three cross sections have the same area. Figure 9 compares the interaction forces vs. displacement for the three cases. It is noted that the PM with a round shape offers the largest force variation, thus the largest stiffness while the PM with the rectangular shape offers the smallest force variation, thus the smallest stiffness.

3.3 Effect of Different Cross-Sectional Shapes of PM on k_{c2}

The magnetic stiffness caused by the interaction between the PM and the core of the electromagnet is found by first finding the flux density of the PM. For an orthorhombic PM $l \times w \times h$, the flux density on the central axis at a distance z from its right face is given as [20]

$$B_{pm} = \frac{\mu_0 M}{\pi} \left[\sin^{-1} \frac{lw}{\sqrt{(l^2 + 4z^2)(w^2 + 4z^2)}} - \sin^{-1} \frac{lw}{\sqrt{[l^2 + 4(z+h)^2][w^2 + 4(z+h)^2]}} \right]. \quad (11)$$

When a ferromagnetic object is placed at an axial location z , the interacting force between the PM and the object is given as [21]

$$F = \alpha AB_{pm}^2 \quad (12)$$

where α is a constant and A is the area of the PM. When the PM magnet placed between the two poles of the electromagnetic core is moved away from the middle of the gap, say to the right, the net force on the PM is given as

$$F = \alpha A(B_{pmr}^2 - B_{pml}^2) \quad (13)$$

where B_{pmr} and B_{pml} are the flux density at the right end and the left end of the core, respectively. In [19], an experiment was conducted to serve two purposes: determine the constant α and compare the actual force and the force predicted by Eq. (13). The constant α was found to be $\alpha = .913 \times 10^6 \text{ mH}^{-1}$ and the forces computed by Eq. (13) agree well with the measured counterparts.

If the cross-sectional shape of the PM changes, it is expected that it will affect k_{c2} . Once again, consider the square shape PM and round shape PM used above. The flux density from a square shape PM can be found by Eq. (11) with $w = l$. Following the derivation procedure given in [20], the equation for the flux density from a round shape PM is obtained as

$$B_{pm} = \frac{\mu_0 M}{2} \left[\frac{z+h}{[r_{pm}^2 + (z+h)^2]^{1/2}} - \frac{z}{[r_{pm}^2 + z^2]^{1/2}} \right] \quad (14)$$

where r_{pm} is the radius of the PM. Figure 10 shows a comparison of the interacting forces caused by the three different shapes of the PMs. It is noted that the round shape results in the largest change in the force, thus the largest k_{c2} while the rectangular shape results in the smallest force variation, thus the smallest k_{c2} . It is also noted that the curve for the round shape PM appears more linear.

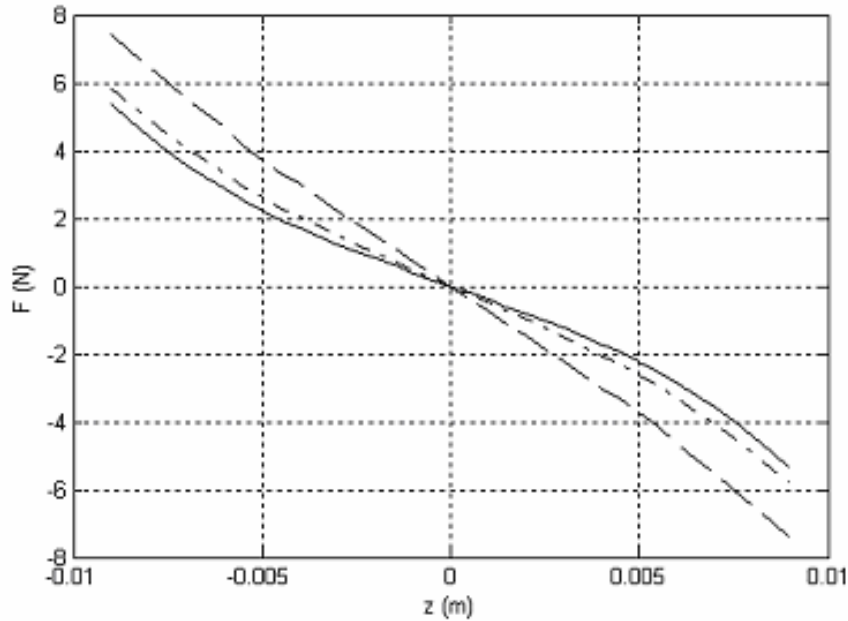


Figure 10. Interaction force of the PM and the core for three different shapes of the PM: solid line, rectangular; dashdot line, square; dashed line, round

3.4 Effect of the Gap Spaces of the Electromagnet on k_v

Consideration of the gap space of the electromagnet is based on several factors: the thickness of the PM, the maximum allowable displacement of the PM, and the size of the electromagnet, etc. With all the other parameters unchanged, two more gap spaces are considered. The interacting forces between the electromagnet and the PM for the three different gap spaces are shown in Fig. 11. It can be seen that with a narrower gap space, a greater and more linear stiffness k_v can be obtained.

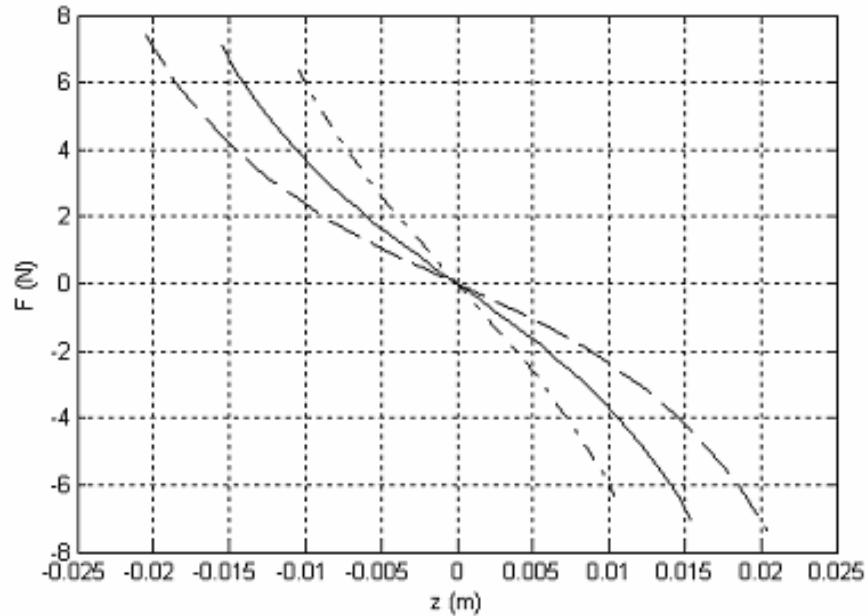


Figure 11. Interacting force between the electromagnet and the PM for three different gap spaces: solid line, $\delta = .042$ m; dashdot line, $\delta = .032$ m; dashed line, $\delta = .052$ m

4. CONCLUSION

Based on this study, the following conclusions can be drawn: 1) In computing the flux density, an electromagnet with a thin layer of coils may be modeled as a current carrying cylindrical sheet. When the difference between the outer radius and the inner radius of the coils increases, the approximation error will increase. 2) A permanent magnet with a round cross section harnesses the flux from the electromagnet most efficiently and offers the greatest magnetic stiffness, as a result, the adjustable margin for k_v is enlarged. 3) A permanent magnet with a round cross section results in the greatest negative constant magnetic stiffness due to the interaction between the permanent magnet and the core of the electromagnet. This effect seems to counteract the effect stated above. However, this counteraction can be compensated by manipulating the constant stiffness created by the absorber beam. 4) In general, the narrower the gap of the electromagnet, the greater and more linear the variable magnetic stiffness.

ACKNOWLEDGEMENT

Financial support for this research was provided by the Natural Sciences and Engineering Research Council of Canada under the grant No. OGP-0184068.

REFERENCES

- [1] M. A. Franchek, M. W. Ryan and R. J. Bernhard, Adaptive passive vibration control, *Journal of Sound and Vibration*, 189 (1995), 565-585.
- [2] K. Nagaya, A. Kurusu, S. Ikai, and Y. Shitani, Vibration control of a structure by using a tunable absorber and an optimal vibration absorber under auto-tuning control, *Journal of Sound and Vibration*, 228 (1999), 773-792.
- [3] N. Varadarajan and S. Nagarajaiah, Response control of building with variable stiffness tuned mass damper using empirical mode decomposition and Hilbert transform algorithm, *16th ASCE Engineering Mechanics Conference*, July 2003, Seattle.
- [4] K. Liu, L. Liao, and J. Liu, Comparison of two auto-tuning methods for a variable stiffness vibration absorber, Accepted for publication in *The Transactions of Canadian Society for Mechanical Engineering*, December 2004.
- [5] W. N. Patten, R. L. Sack, and Q. He, Controlled semiactive hydraulic vibration absorber for bridges, *Journal of Structural Engineering*, 122 (1996), 87-192.
- [6] M. D. Symans and M. C. Constantinou, Seismic testing of a building structure with a semi-active fluid damper control system, *Earthquake Engineering and Structural Dynamics*, 26 (1997), 759-777.
- [7] P. Dupont, P. Kasturi, and A. Stokes, Semi-active control of friction dampers, *Journal of Sound and Vibration*, 202 (1997), 203-218.
- [8] L. Y. Lu, Semi-active modal control seismic structures with variable friction dampers, *Engineering Structures*, 26 (2004), 437-454.
- [9] S. B. Choi, H. K. Lee, and E. G. Chang, Field test results of a semi-active ER suspension system associated with skyhook controller, *Mechatronics*, 11 (2001), 345-353.
- [10] A. Milecki, Investigation and control of magneto-rheological fluid dampers, *International Journal of Machine Tools & Manufacture*, 41 (2001), 379-391.
- [11] B. Erkus, M. Abe, and Y. Fujino, Investigation of semi-active control for seismic protection of elevated highway bridges, *Engineering Structures*, 24 (2002), 281-293.
- [12] T. Mizuno and K. Araki, Control system design of a dynamic vibration absorber with an electromagnetic servomechanism, *Mechanical Systems and Signal Processing*, 7 (1993), 293-306.
- [13] M. S. Trimboli, R. Wimmel, and E. Breitbach, A quasi-active approach to vibration isolation using magnetic springs, *SPIE*, 2193 (1994), 73-83.
- [14] Y. Matsuzaki, T. Ikeda, A. Nae, and T. Sasaki, Electromagnetic forces for a new vibration control system: experimental verification, *Smart Materials and Structures*, 9 (2000), 127-131.
- [15] C. C. Chen and M. K. Yeh, Parametric instability of a beam under electromagnetic excitation, *Journal of Sound and Vibration*, 240 (2001), 747-764.
- [16] S. Yashita and K. Seto, Vibration and noise control using dual dynamic absorbers with magnetic damping, *Proceedings of The Third International ISEM Symposium on the Application of Electromagnetic Forces*, Sendai, 1992.
- [17] D. Kienholz and S. Pendleton, Demonstration of solar array vibration suppression, *SPIE*, 2193 (1994), 59-72.
- [18] K. Liu, J. Liu, and L. Liao, Application of a tunable electromagnetic damper in suppression of structural vibration, Submitted to *The Transactions of the Canadian Society for Mechanical Engineering*, October 2004
- [19] J. Liu and K. Liu, A tunable electromagnetic vibration absorber: characterization and application, submitted to *The Journal of Sound and Vibration*, January 2005.
- [20] D. J. Craik, *Magnetism: Principles and Applications*. Chichester, New York, Wiley, 1995.
- [21] H. H. Woodson and J. R. Melcher, *Electromechanical Dynamics—Part I: Discrete Systems*, John Wiley & Sons, 1968.